

# Absorption/Expulsion of Oligomers and Linear Macromolecules in a Polymer Brush

A. Milchev<sup>\*1,3</sup>, S. A. Egorov<sup>2</sup> and K. Binder<sup>1</sup>

<sup>1</sup> *Institut für Physik, Johannes Gutenberg-Universität, D-55099 Mainz, Germany,* <sup>2</sup> *Department of Chemistry, University of Virginia, Charlottesville, Virginia 22901, USA,* <sup>3</sup> *Institute of Physical Chemistry, Bulgarian Academy of Sciences, 1113 Sofia, Bulgaria*

The absorption of free linear chains in a polymer brush was studied with respect to chain size  $L$  and compatibility  $\chi$  with the brush by means of Monte Carlo (MC) simulations and Density Functional Theory (DFT) / Self-Consistent Field Theory (SCFT) at both moderate,  $\sigma_g = 0.25$ , and high,  $\sigma_g = 1.00$ , grafting densities using a bead-spring model. Different concentrations of the free chains  $0.0625 \leq \phi_o \leq 0.375$  are examined.

Contrary to the case of  $\chi = 0$  when all species are almost completely ejected by the polymer brush irrespective of their length  $L$ , for  $\chi < 0$  we find that the degree of absorption (absorbed amount)  $\Gamma(L)$  undergoes a sharp crossover from weak to strong ( $\approx 100\%$ ) absorption, discriminating between oligomers,  $1 \leq L \leq 8$ , and longer chains. For a moderately dense brush,  $\sigma_g = 0.25$ , the longer species,  $L > 8$ , populate predominantly the deep inner part of the brush whereas in a dense brush  $\sigma_g = 1.00$  they penetrate into the “fluffy” tail of the dense brush only. Gyration radius  $R_g$  and end-to-end distance  $R_e$  of absorbed chains thereby scale with length  $L$  as free polymers in the bulk. Using both MC and DFT/SCFT methods for brushes of different chain length  $32 \leq N \leq 256$ , we demonstrate the existence of unique *critical* value of compatibility  $\chi = \chi^c < 0$ . For  $\chi^c(\phi_o)$  the energy of free chains attains the *same* value, irrespective of length  $L$  whereas the entropy of free chain displays a pronounced minimum. At  $\chi^c$  all density profiles of absorbing chains with different  $L$  intersect at the same distance from the grafting plane.

The penetration/expulsion kinetics of free chains into the polymer brush after an instantaneous change in their compatibility  $\chi$  displays a rather rich behavior. We find three distinct regimes of penetration kinetics of free chains regarding the length  $L$ : I ( $1 \leq L \leq 8$ ), II ( $8 \leq L \leq N$ ), and III ( $L > N$ ), in which the time of absorption  $\tau$  grows with  $L$  at a different rate. During the initial stages of penetration into the brush one observes a power-law increase of  $\Gamma \propto t^\alpha$  with power  $\alpha \propto -\ln \phi_o$  whereby penetration of the free chains into the brush gets *slower* as their concentration rises.

Keywords:

## I. INTRODUCTION

Densely-grafted chains on nonadsorbing substrate surfaces form the so-called “polymer brush” [1–16]. These systems find various important applications [16], e.g. as lubricants [12], for colloid stabilization [17], for tuning of adhesion and wetting properties [16, 18], for improving the biocompatibility of drugs [19], as protective coatings preventing protein adsorption (“nonfouling” surfaces) in a biological milieu [20], microfluidic chips for biomolecule separation [21], etc.

The theoretical description of the conformations of macromolecules in these polymer brushes and their dynamics has been an active topic of research hitherto (e.g., [22–28]; for early reviews see [9–15]). Also the interaction of the brushes with either the solvent molecules (e.g. [23, 25]) or globular proteins [24] and/or other nanoparticles (e.g., [22, 26, 29–33]) has found much recent attention. However, in many situations of interest there will also occur free polymer chains in the solution, interacting with the polymers of the brush. This interaction has received relatively less attention, apart from the case where a polymer brush interacts with a dense polymer melt [2, 34–43]. The latter case is particularly interesting because there is very little interpenetration of the grafted chains in the melt and the free chains in the brush even if their chemical nature is identical (“wetting autophobicity” [44–47]).

In contrast, scaling theory [2], self-consistent field [48] and simulation [49] have predicted partial penetration of free chains into moderately dense brushes of identical chemical nature in semi-dilute solutions when the monomer volume fraction in solution approaches that of the brush, and this behavior has been confirmed experimentally [43]. Of course, when the polymer solution is very dilute, the brush provides a free energy barrier for penetration of free chains into it and this limits the grafting density that can be achieved when one prepares a brush by grafting chains from solution [16] (see also some attempts to model this process by simulations [50, 51]). Similarly, since typically the energy won by the chain end when it gets grafted is of the order of  $10k_B T$  only [10, 12, 16], there is a nonzero probability that brush chains get released from the grafting substrate surface and are subsequently expelled from the

---

\* Corresponding author email: milchev@ipc.bas.bg

brush [52].

However, most cases studied so far refer to the situation that (apart from chain end effects) the chains in the bulk and those in the solution are identical. It is interesting, therefore, to consider the more general situation when the grafted chains and those in the bulk differ in their chemical nature. Then the problem of compatibility (traditionally modelled by introducing a Flory-Huggins  $\chi$ -parameter [53]) between the two types of chains arises. Then, there is also no reason to assume that the length  $N$  of the grafted chains, and the length  $L$  of the free chains are equal. Such situations (in particular, when the grafted and the free chains attract each other,  $\chi < 0$ ) are of great interest for modern applications such as protein adsorption, "antifouling" surfaces [20], etc. However, to the best of our knowledge, no systematic study of the effects of the various parameters ( $N$ ,  $L$ ,  $\chi$  and monomer concentration of the free chains  $\phi_o$ ) on the amount of absorption and the penetration kinetics has been reported so far. The present paper presents simulation and Density Functional Theory (DFT) results in an effort to fill this gap. In Section II we describe the model and comment on some simulation aspects; Section III summarizes our theoretical approach which includes both static and dynamic versions (DDFT) of DFT as well as Self-Consistent Field Theory (SCFT) calculations. The numerical results are described in Section IV while Section V contains a summary and discussion.

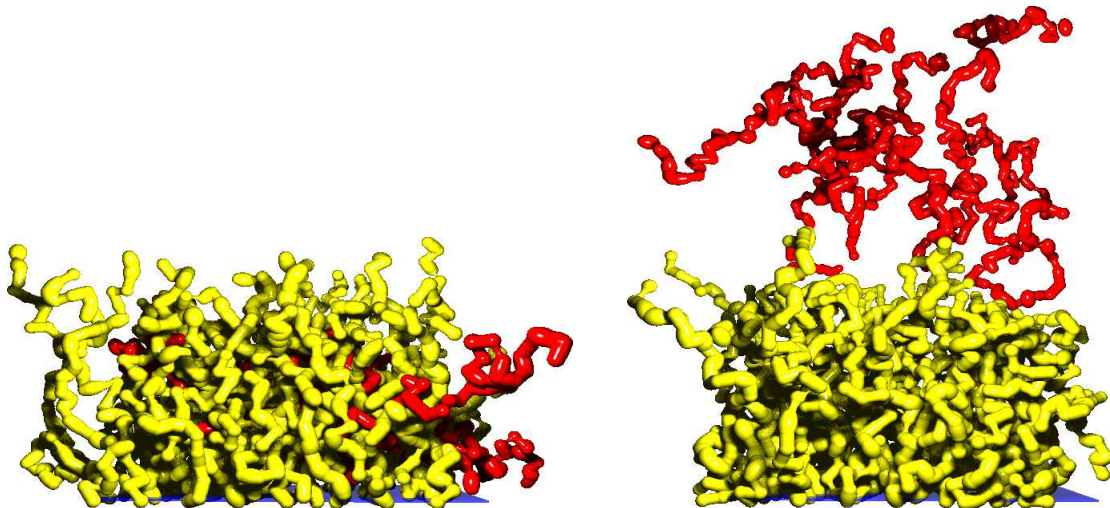


FIG. 1: Snapshots of a polymer brush with chain length  $N = 32$  at grafting density  $\sigma_g = 0.25$  and free chains of length  $L = 32$  at equilibrium: (left) absorption at  $\epsilon_{po} = 2.00$ , and (right) expulsion at  $\epsilon_{po} = 0.01$ .

## II. MODEL AND SIMULATION ASPECTS

We have used a coarse grained off-lattice bead spring model[55, 56] to describe the polymer chains in our system. As far as for many applications in a biological context rather short grafted chains are used [57], we restrict ourselves to length  $N = 32$  of the grafted chains. The polymer brush consists of linear chains of length  $N$  grafted at one end to a flat structureless surface. The effective bonded interaction is described by the FENE (finitely extensible nonlinear elastic) potential,

$$U_{FENE} = -K(l_{max} - l_0)^2 \ln \left[ 1 - \left( \frac{l - l_0}{l_{max} - l_0} \right)^2 \right] \quad (1)$$

with  $K = 20$ ,  $l_{max} = 1$ ,  $l_0 = 0.7$ ,  $l_{min} = 0.4$ . Thus the equilibrium bond length between nearest neighbor monomers is  $l_0 = 0.7$ . Here and in what follows we use the maximal extension of the bonds,  $l_{max} = 1$ , as our unit length while the potential strength is measured in units of thermal energy  $k_B T$  where  $k_B$  is the Boltzmann constant.

The nonbonded interactions between brush and free chain segments are described by the Morse potential,

$$\frac{U_M(r)}{\epsilon_M} = \exp[-2\alpha(r - r_{min})] - 2 \exp[-\alpha(r - r_{min})], \quad (2)$$

with  $\alpha = 24$ ,  $r_{min} = 0.8$ , and  $\epsilon_M/k_B T$  standing for the strength of brush-brush,  $\epsilon_{pp}$ , polymer-polymer,  $\epsilon_{oo}$ , and brush-polymer,  $\epsilon_{po}$  interactions. In our present study we take typically  $\epsilon_{pp} = 0.2$ ,  $\epsilon_{oo} = 0.1$  (that is, in the good solvent regime with only excluded volume interactions). For  $\epsilon_{po} = 2.00$ ,  $\chi = -1.85$  the free chains are absorbed in the brush whereas for  $\epsilon_{po} = 0.01$ ,  $\chi = -0.005$  the polymer brush ejects them into the bulk. Note that we define here the compatibility parameter  $\chi$  simply as  $\chi = 0.5(\epsilon_{pp} + \epsilon_{oo}) - \epsilon_{po}$ , and do not include the coordination number (which is done when one uses lattice models [53]).

The size of the container is  $16 \times 16 \times 32$ . The polymer chains are tethered to grafting sites which constitute a triangular periodic lattice on the substrate whereby the closest distance between grafting sites is  $l_{max} = 1$ . Thus the largest grafting density  $\sigma_g = 1.0$  involves 8192 brush segments, if the polymer chains are anchored at distance  $l_{max} = 1$ , and  $\sigma_g = 0.25$ , i.e., 2048 brush segments, if the 'lattice constant', i.e., the distance between adjacent head monomers on the surface is equal to  $2l_{max}$ . Note that  $\sigma = 1.0$  corresponds to a simulation where the monomer density in the brush near the wall is close to the density of a polymer melt while  $\sigma = 0.25$  would correspond to a rather concentrated polymer solution.

For the chain model,  $\epsilon_M/k_B T = \epsilon_{pp} = 0.2$  corresponds to good solvent conditions since the Theta-point for a (dilute) solution of polymers described by the model, Eqs. 1-2 has been estimated[55] as  $k_B \Theta / \epsilon_M = 0.62$ . In all our simulations we use brushes formed by polymer chains consisting of  $N = 32$  effective monomers whereas the number of free chains  $N_o$  of length  $L$  (where  $L$  spans the interval  $1 \leq L \leq 64$ ) is taken such that the total number of free chain segments remains constant and is equal to 512. For a certain length  $L = 64$ , however, we also change the concentration of free chains in the container by varying their number  $N_o$  in the interval  $8 \leq N_o \leq 48$ . Thus, the volume fraction  $c_o$  of 64-free chains is varied between  $0.0625 \leq c_o \leq 0.5$ . Note that, as usual, solvent molecules are not explicitly included [56, 58, 59] but work which includes solvent explicitly [23] would yield very similar results.

For a dense brush with polymer chains of lengths  $N = 32$  statistical averages were derived from typically  $10^7$  Monte Carlo Steps (MCS) per monomer. The Monte Carlo algorithm consists of attempted moves whereby a monomer is chosen at random and one attempts to displace it to a new randomly chosen position  $-0.5 \leq \Delta x, \Delta y, \Delta z \leq 0.5$  regarding the old position. We use periodic boundary conditions in the  $x - y$  directions and impenetrable hard walls in the  $z$  direction. Two typical configurations of the polymer brush with free chains of length  $L = 32$ , are shown in Fig. 1 for the case of good,  $\epsilon_{po} = 2.00$ , and poor,  $\epsilon_{po} = 0.01$ , compatibility with the polymer brush.

### III. THEORY

We employ classical DFT to compute density profiles of free and grafted polymer chains. Theory has been discussed in detail in previous publications, so here we briefly summarize its most important aspects. The starting point of the DFT treatment is the expression for the grand free energy,  $\Omega$ , as a functional of the density profiles of free and grafted chains,  $\phi_o(\mathbf{R}_o)$  and  $\phi_p(\mathbf{R}_p)$ , respectively ( $\mathbf{R}_{p/o} = \{\mathbf{r}_i\}$ , where  $\mathbf{r}_i$  are the positions of the chain segments). The functional  $\Omega$  is related to the Helmholtz free energy functional,  $F$ , via a Legendre transform:[60, 61]

$$\Omega[\phi_o(\mathbf{R}_o), \phi_p(\mathbf{R}_p)] = F[\phi_o(\mathbf{R}_o), \phi_p(\mathbf{R}_p)] + \sum_{\alpha=o,p} \int d\mathbf{R}_\alpha \phi_\alpha(\mathbf{R}_\alpha) V_\alpha(\mathbf{R}_\alpha), \quad (3)$$

where  $V_\alpha(\mathbf{R}_\alpha)$  is the external field, which in the present case is due to the hard-sphere like interaction of the polymer segments with the hard wall,  $V_p(\mathbf{R}_p) = \sum_{i=1}^N v_p(z_i)$ , where  $v_p(z_i) = \infty$  for  $z \leq 0$  and  $v_p(z_i) = 0$  otherwise, with analogous expression holding for  $V_o(\mathbf{R}_o)$ . Additionally, the innermost ( $i = 1$ ) bead of each grafted chain is tethered to the wall via a grafting potential  $\exp[-\beta v_p(z_1)/k_B T] = \delta(z_1)$ , where  $\beta = 1/k_B T$ . Note that the chemical potential of both free and grafted chains is absent from the second term of Eq. (3) because the DFT calculations are performed at a fixed number of both free and grafted segments in order to mimic the MC simulations:  $\int_0^{z_{max}} dz \phi_p(z) = \sigma_g N$  and  $\int_0^{z_{max}} dz \phi_o(z) = N_o L / A$ . in the above,  $z_{max} = 32$  is the box length and  $A = 256$  is the wall area.

The Helmholtz free energy functional is separated into ideal and excess parts,[60, 61] with the former given by:

$$\beta F_{id}[\phi_o(\mathbf{R}_o), \phi_p(\mathbf{R}_p)] = \sum_{\alpha=o,p} \left\{ \int d\mathbf{R}_\alpha \phi_\alpha(\mathbf{R}_\alpha) [\ln \phi_\alpha(\mathbf{R}_\alpha) - 1] + \beta \int d\mathbf{R}_\alpha \phi_\alpha(\mathbf{R}_\alpha) V_b(\mathbf{R}_\alpha) \right\}. \quad (4)$$

where the bonding energy  $V_b$  for the grafted chains is taken as follows:

$$\exp[-\beta V_b(\mathbf{R}_g)] = \prod_{i=1}^{N-1} \frac{\delta(|\mathbf{r}_i - \mathbf{r}_{i+1}| - b_l)}{4\pi b_l^2}, \quad (5)$$

with a similar expression for free chains, with  $N$  replaced by  $L$ . This bonding potential constrains adjacent segments to a fixed separation  $b_l$ .

The excess part of the Helmholtz free energy is written as a sum of repulsive (hard chain) and attractive terms, with the former computed in the weighted density approximation and the latter obtained within mean-field approach, using Eqs. (12)-(17) from Ref. [25]; for the sake of brevity we do not reproduce these equations here.

The minimization of the grand free energy functional with respect to  $\phi_p(\mathbf{R}_p)$  yields the equilibrium density distribution for the grafted chains which can be integrated over grafting and bonding delta-functions to obtain the following result for the density profile of the  $i$ th segment of the grafted chains:[25]

$$\phi_{pi}(z) = C_i I_p(z) I_i^-(z) I_i^+(z), \quad (6)$$

where

$$I_p(z) = \exp[-\beta(v_p(z) + \lambda_p(z))], \quad (7)$$

with

$$\lambda_p(z) = \frac{\delta F_{ex}}{\delta \phi_p(z)}. \quad (8)$$

The two propagators in Eq. (6),  $I_i^+$  and  $I_i^-$  move from the free ( $i = N$ ) and the tethered ( $i = 1$ ) ends of the chain, respectively. They are computed via recursive relations given by Eqs. (23)-(25) of Ref. [25].

The normalization constant  $C_i$  in Eq. (6) is chosen to ensure that the  $i$ th segment density profile is normalized to  $\sigma_g$ . The total segment density profile for the grafted chains is given by:

$$\phi_p(z) = \sum_{i=1}^N \phi_{pi}(z). \quad (9)$$

The equilibrium density profile for the segments of the free chains can be obtained in a similar way, by minimizing the grand free energy functional with respect to  $\phi_o(\mathbf{R}_o)$  and integrating over bond-length constraining delta functions.

The DFT equations described above are solved simultaneously to obtain the segment density profiles for free and grafted chains. The equations are solved iteratively using Picard algorithm,[25] with the step size along the  $z$  coordinate taken to be 0.0325. The above procedure yields equilibrium segment density profiles for a given set of interaction potentials. In addition to the equilibrium structural properties, we have also studied the kinetics of the adsorption of free chains into the brush, following a switch of the interaction potential between free and grafted segments from repulsive to attractive. To this end, we have employed the DDFT method, which is a dynamical generalization of the DFT approach.[63, 64] MC simulations have indicated that the segment density profiles of the grafted chains are essentially independent of the strength of the attraction between free and grafted segments. Accordingly, in our DDFT calculations we take  $\phi_p(z)$  to be time independent and focus on the time dependence of the free chain density,  $\phi_o(z, t)$ .

The time evolution of the segment density profile of free chains is given by the following equation:[64]

$$\frac{\partial \phi_o(z, t)}{\partial \tau} = \frac{\partial}{\partial z} \phi_o(z, t) \frac{\partial}{\partial z} \beta \mu(z, t), \quad (10)$$

where  $\mu(z, t)$  is the non-equilibrium local chemical potential, and dimensionless time  $\tau$  is defined according to  $\tau = k_B T M / l_{max}^2 t$ , where  $M$  is the mobility coefficient.

Initial density profile  $\phi_o(z, t = 0)$  corresponds to the equilibrium distribution of free chains at a repulsive brush, i.e.  $\epsilon_{po} = 0.01$ . At  $t = 0$ , the brush-free polymer attraction is instantaneously “switched on”, i.e. we set  $\epsilon_{po} = 2$ . The time-dependent polymer density profile is then propagated according to the Eq. (10), with the time-dependent chemical potential given by:

$$\beta \mu(z, t) = \ln \phi_o(z, t) - \ln \sum_{i=1}^L C_i I_o(z, t) I_i^-(z, t) I_i^+(z, t), \quad (11)$$

where  $I_o(z, t)$  is obtained by substituting the time-dependent density  $\phi_o(z, t)$  into the expression for  $I_o(z)$  (and likewise for the propagators  $I_i^-(z, t)$  and  $I_i^+(z, t)$ ). We solve Eq. (10) using Crank-Nicholson scheme.[63, 64] Note that Eq. (10) has the form of a continuity equation with the flux (current density) given by  $j(z, t) = -\phi_o(z, t) \frac{\partial}{\partial z} \beta \mu(z, t)$ . The fact that the DDFT method propagates  $\phi_o(z, t)$  via a continuity-type equation guarantees the conservation of the total number of segments in the system, which is consistent with the simulation set-up.

In order to compare the results of the DDFT approach with kinetic MC data, we set the mobility coefficient  $M$  equal to unity and adjust the conversion factor between DDFT dimensionless time and kinetic MC number of steps

for one particular set of parameters  $L$  and  $\phi_o$ . Comparisons for all other values of  $L$  and  $\phi_o$  are performed using the same conversion factor, while assuming  $M$  to be inversely proportional to both  $L$  and  $\phi_o$ .

With the goal of shedding further light on the thermodynamic aspects of the adsorption process, we have also performed self-consistent field theory (SCFT) calculations of the structural properties as a function of the interaction strength between the segments of the brush and the free chains (in SCFT approach this interaction is characterized by the parameter  $\chi$  which is calculated in the standard fashion from the corresponding potential well-depths:  $\chi = 0.5 * (\epsilon_{pp} + \epsilon_{oo}) - \epsilon_{po}$ ). The main motivation behind carrying out SCFT calculations is the fact that this approach provides a more straightforward way to decompose the free energy into entropic and energetic components, thereby providing a complementary (to DFT) view of the adsorption process.

The basic equations of the SCFT method are well known,[42, 48] and will not be reproduced here for the sake of brevity. Once again, the density profiles for free and grafted chains are written in terms of the propagators, the only major difference from the DFT approach being that instead of the equation of state, one employs the incompressibility constraint to set up the equations for the density profiles, which are once again solved iteratively using Picard's method. For example, the equation for the density profile of the grafted chain segments takes the form:

$$\phi_p(z) = C_p \sum_{i=1}^N \frac{I_i^-(z)I_i^+(z)}{G_p(z)}, \quad (12)$$

where the normalization constant  $C_p$  is obtained from the grafting density  $\sigma_g$ , and  $G_p(z) = \exp(-\beta u_p(z))$ , with  $\beta u_p(z) = u'(z) + \chi_{po}\phi_o(z)$ . The hard core potential  $u'$  is independent of the segment type and serves as a Lagrange multiplier enforcing the incompressibility condition, meaning that the lattice space is completely filled and no segment overlap occurs. The density profile of the free chain segments is obtained in a similar way.

Once the profiles are calculated, one can easily obtain excess entropy and energy of the free chains (relative to pure unmixed components) as follows [65]:

$$S - S^* = -k_B \int_0^{z_{max}} dz \phi_o(z) \left\{ \frac{\ln \phi_o^b}{L} + \ln G_o(z) \right\}, \quad (13)$$

$$U - U^* = -k_B T \int_0^{z_{max}} dz \phi_o(z) \chi_{po} \phi_p(z), \quad (14)$$

where  $\phi_o^b$  is the bulk volume fraction of free chains.

## IV. RESULTS

### A. Equilibrium properties

In Fig. 2 we show the density profiles of the free chains,  $\phi_o(z)$ , of length  $L$  for an attractive,  $\epsilon_{po} = 2.00$ , and a neutral,  $\epsilon_{po} = 0.04$ , brush along with the monomer density profile of the brush itself,  $\phi_p(z)$ . Our MC simulation results indicate that at fixed segment concentration,  $c_i$ , the brush profile,  $\phi_p(z)$ , is virtually insensitive to  $L$ , whereupon we keep only one such profile in the graphs. The most striking feature which may be concluded from Fig. 2 is, somewhat counter-intuitively, the strong increase of absorption with growing length of the absorbed free chains  $L$ . Evidently, both at moderate,  $\sigma_g = 0.25$ , and high,  $\sigma_g = 1.00$ , grafting density, the longer polymers are entirely placed inside the polymer brush whereas the much more mobile short species  $L < 8$  remain uniformly distributed in the bulk above the brush end. Since some of the absorbing chains with larger  $L$  get stuck inside the brush, their density profiles could not smoothen sufficiently for the time of the simulation run. Therefore, we observe rather large statistical fluctuations in  $\phi_o(z)$ . For repulsive brushes all species are largely expelled from the brush whereby the situation is reversed as far as the free chain length  $L$  is concerned. In the very dense brush  $\sigma_g = 1.0$ , the brush profile displays the typical oscillations near the grafting surface suggesting some layering immediately in the vicinity of the grafting wall - Fig. 2c,d. In all graphs one observes pronounced depletion effects at the upper container wall, opposing the brush. However, the inhomogeneity of  $\phi_o(z)$  near the wall at  $z = 32$  has no effect on  $\phi_o(z)$  in the region of the polymer brush, the flat part of  $\phi_o(z)$  in between the brush and the confining wall at  $z = 32$  is broad enough to eliminate any finite-size effects associated with the finite linear dimension of the simulation box in  $z$ -direction.

One should note also the good agreement between simulation and DFT results. In fact, the thin lines, indicating the latter, may hardly be distinguished from the Monte Carlo data (thick lines) in Fig. 2a,b. The only significant discrepancy between theory and simulation is observed in the brush profile in the vicinity of the grafting wall, where

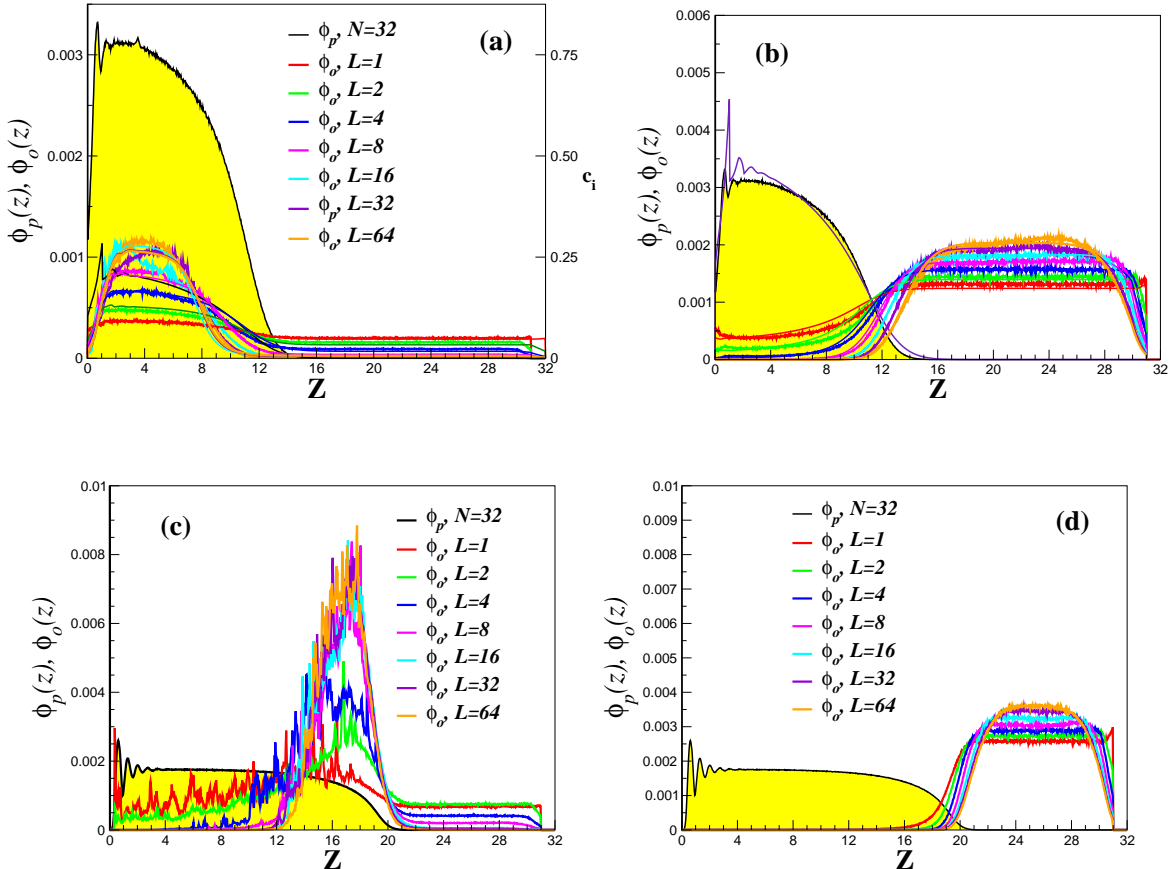


FIG. 2: Density profiles of the polymer brush,  $\phi_p(z)$ , (shaded area) and of free chains,  $\phi_o(z)$ , (thin lines) of length  $L$ , (given as parameter) at two grafting densities:  $\sigma_g = 0.25$  (upper row), and  $\sigma_g = 1.00$  (lower row). (a) and (c) illustrate good compatibility between brush and free chains,  $\epsilon_{po} = 2.0$  while (b) and (d) demonstrate a case of bad compatibility,  $\epsilon_{po} = 0.04$ . Thin solid lines in (a) and (b) denote results from the DFT calculation. The densities in (a) are normalized so as to reproduce the correct ratio of brush to free chains concentrations  $\phi_p$  and  $\phi_o$  (the absolute particle concentration  $c_i$  is indicated in the alternative  $y$ -axis. For the sake of better visibility, in (b), (c), and (d) the density of all species is normalized to unit area.

DFT approach overestimates the oscillations. This discrepancy is likely due to the fact that in the DFT method the bond lengths are constraint via delta-functions to a constant value of  $b_l = 0.75$ , while in the simulations the bonds are allowed to vibrate under FENE potential, Eq. (1). For  $L = 64$ , Fig. 3 shows a qualitatively similar behavior of the density profiles for the cases of gradually increasing free chain concentration (indicated by the number of free chains  $\mathcal{N}_o$  as parameter). Expectedly, for  $\mathcal{N}_o \geq 24$  (which corresponds to monomer concentration  $c_i = 0.1875$ ) and  $\sigma_g = 0.25$ , the free chains are present in the bulk over the brush as the brush interior is then entirely filled. However, when the brush - free chain attraction increases to  $\epsilon_{po} = 3.00$ , the MC data (not shown here) indicate complete absorption of the free chains into the brush with virtually no free chains in the bulk above the polymer brush even at the highest concentration of  $c_i = 0.375$ .

With increasing grafting density and/or free chain concentration, the agreement between DFT and MC deteriorates somewhat, with the theory underestimating the degree of penetration of free chains into the brush (see discussion of Fig. 5 below), which is likely due to the simple Tarazona's weighting function employed in our DFT calculations. It is well known that at higher densities it would be more appropriate to use weighting functions from the Fundamental Measure Theory.[66] Indeed, precisely such approach has been recently used to study adsorption and retention of spherical particles in polymer brushes [54].

Next, we present MC and DFT results for the absorbed amount of free chains as a function of degree of polymerization and concentration. The absolute absorbed amount is defined as the number of polymer segments located "inside the brush", namely, in the region  $z < z_{cut}$ , where the cutoff distance  $z_{cut}$  is defined in such a way that 99% of the brush segments are located in the region  $z < z_{cut}$ . The *relative* absorbed amount  $\Gamma$  is defined as the ratio

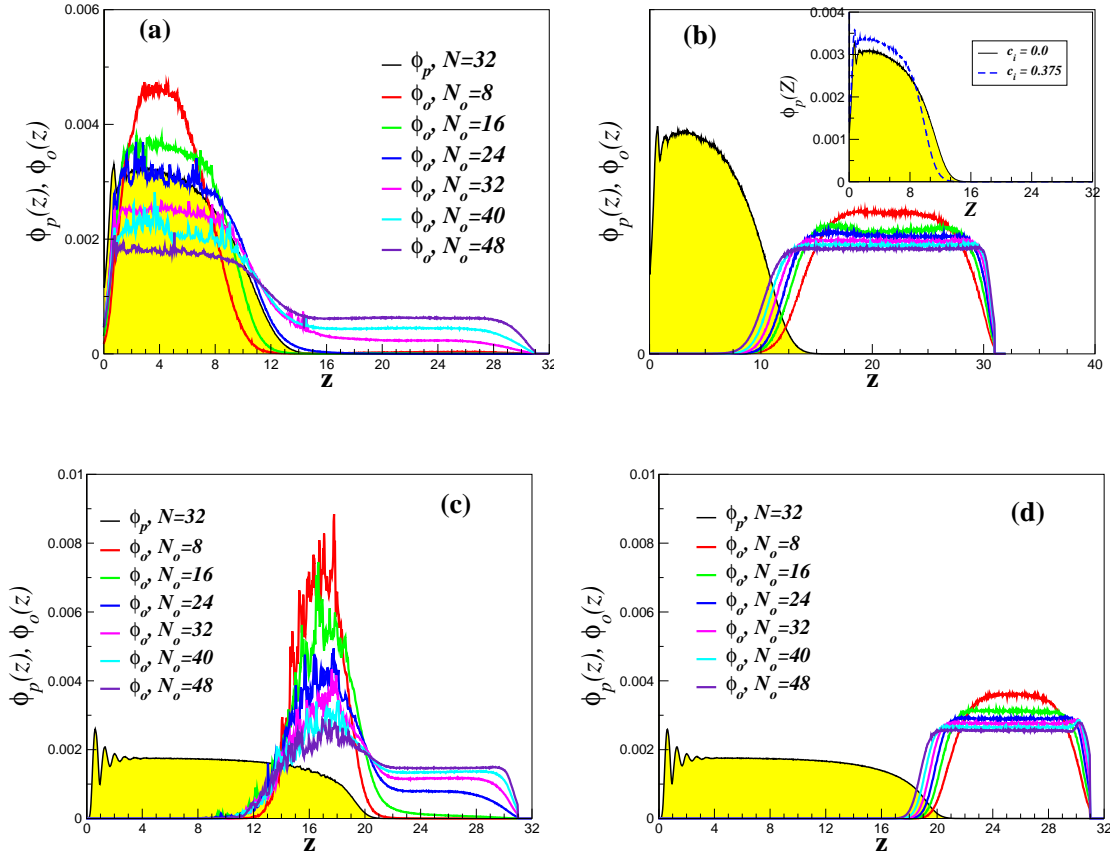


FIG. 3: Density profiles of the polymer brush,  $\phi_p(z)$ , (shaded area) and of free chains,  $\phi_o(z)$ , (thick lines) of length  $L = 64$  for different free chain concentration (number of free chains  $N_c$ ) (given as parameter) at two grafting densities:  $\sigma_g = 0.25$  (upper row), and  $\sigma_g = 1.00$  (lower row). Thin lines in (a) denote DFT results. The inset in (b) shows the change in the density profile of brush monomers for two values of free chain concentration:  $c_i = 0.00$ , and  $0.375$ . In (a), (c) and (d)  $\phi_p$  stays practically constant.

of the absolute adsorbed amount to the total number of free chain segments. In Fig. 4a one may observe the steep increase in  $\Gamma$  with growing polymer length  $L$  both for brushes with  $\sigma_g = 0.25$  and  $\sigma_g = 1.00$  when  $\epsilon_{po} = 2.0$ . Indeed, as indicated also in Fig. 2, as soon as  $L \geq 8$ , the adsorbed amount saturates at nearly 90%. A much more gradual growth of  $\Gamma$  is found for the *critical* attraction  $\epsilon_{po} = 1.70$  (see below). In Fig. 4a one sees again that DFT results for the adsorbed amount of polymers as a function of the adsorbate polymerization index (shown here for the case of lower grafting density) are in good agreement with MC data, with the exception of the intermediate-length chains, where DFT overestimates the adsorbed amount somewhat.

Especially interesting is the observation, Fig. 4b, that the conformations of the absorbed chains inside the brush practically do not change with respect to those of the free chains in the bulk - the scaling behavior of the parallel and perpendicular components of the end-to-end (squared) distance  $R_e^2$  and radius of gyration,  $R_g^2$ , is demonstrated in logarithmic coordinates by straight lines whereby the value of the Flory exponent  $\nu \approx 0.64$ . Due to the short lengths of the free chains used here this value is slightly larger than what is expected for very long chains (namely  $\nu = 0.59$ ). Only the absorbed chains that are longer than the polymers of the brush,  $L = 64 > N = 32$ , indicate deviations from the scaling law of single polymers with excluded-volume interactions: the parallel component  $R_{gxy}$  slightly exceeds, and the perpendicular component,  $R_{gz}$ , falls below the straight line suggesting that the original shape of the  $L = 64$  coil flattens parallel to the grafting plane.

Fig. 5 displays the dependence of adsorbed amount of polymers on the concentration for the highest polymerization index studied,  $L = 64$ . One sees that for both grafting densities the total number of adsorbed monomers increases with concentration, while the relative adsorbed amount decreases. DFT results (again presented for the case of lower

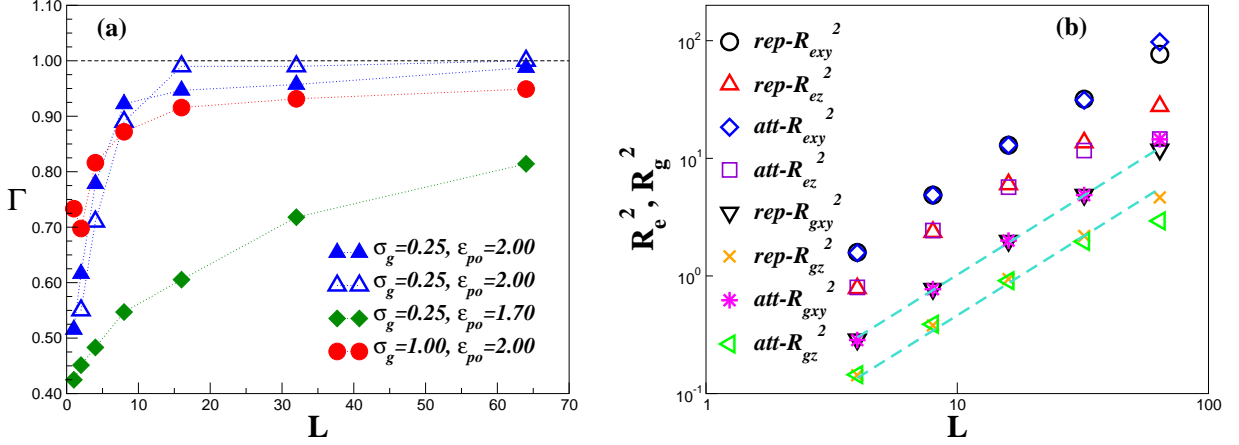


FIG. 4: (a) Variation of the absorbed amount  $\Gamma$  with polymerization index  $L$  of the free chains for two grafting densities. Empty symbols denote DFT results. The case  $\epsilon_{po} = 1.70$  refers to the *critical* degree of brush-polymer compatibility (cf. Section IV B). (b) Mean squared radius of gyration,  $R_{gxy}^2$ , and end-to-end distance,  $R_{exy}^2$ , parallel and perpendicular,  $R_{gz}^2$ ,  $R_{ez}^2$  to the grafting plane against length of the free chains  $L$  at grafting density  $\sigma_g = 0.25$ . Dashed lines denote the observed slope  $\approx 1.28 \pm 0.03$ . Only for the longest free chains with  $L = 64$  a marked deviation from the standard scaling behavior may be detected.

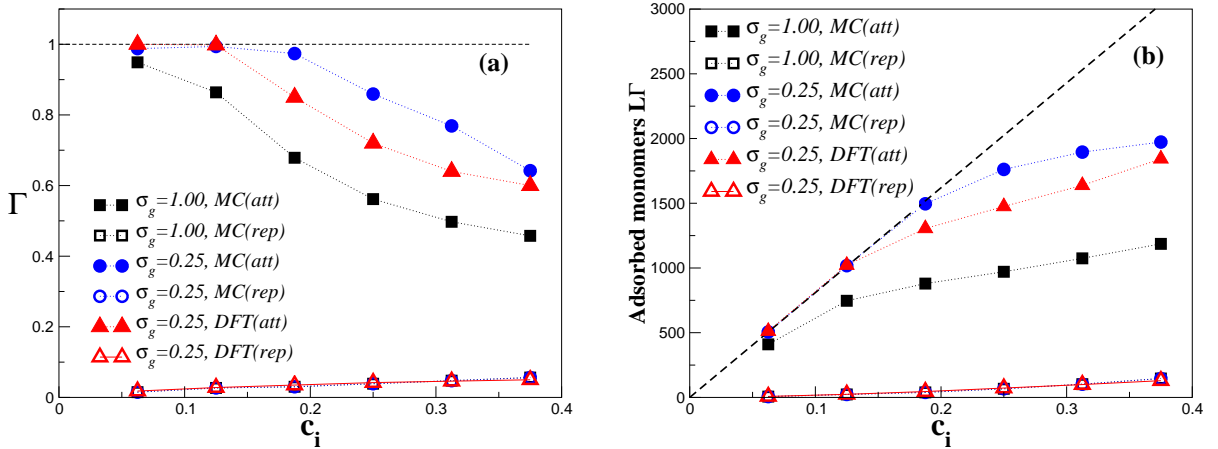


FIG. 5: Variation of the absorbed amount  $\Gamma$  with free chain concentration  $c_i$  for  $L = 64$  and two grafting densities:  $\sigma_g = 0.25$  (circles), and  $\sigma_g = 1.00$  (squares). Full symbols correspond to polymer absorption with  $\epsilon_{po} = 2.0$  and empty symbols denote expulsion  $\epsilon_{po} = 0.01$ . (a) Absorbed fraction vs.  $c_i$ , (b) Total number of adsorbed monomers against  $c_i$ .

grafting density) fall below MC data at higher concentrations, illustrating the aforementioned observation that DFT underestimates the degree of penetration of free chains into the brush at higher concentrations.

## B. The critical compatibility $\chi^c$

As a remarkable feature of polymer absorption in a brush we find the existence of a *critical* degree of compatibility  $\chi^c$  between the grafted and free chains. Fig. 6a displays brush and free chain density profiles for various polymer chain lengths at the critical value of the brush-polymer attraction strength ( $\epsilon_{po}^c = 1.70$  for MC simulations and  $\chi_{po}^c = -1.40$  for SCFT calculations). While simulation and theoretical results differ quantitatively, there is a striking qualitative similarity in that the density profiles, irrespective of the length  $L$  of the free chains, all intersect in two single points (inside and outside the brush). The DFT approach produces exactly the same behavior albeit for a smaller  $\epsilon_{po}^c = 1.0$



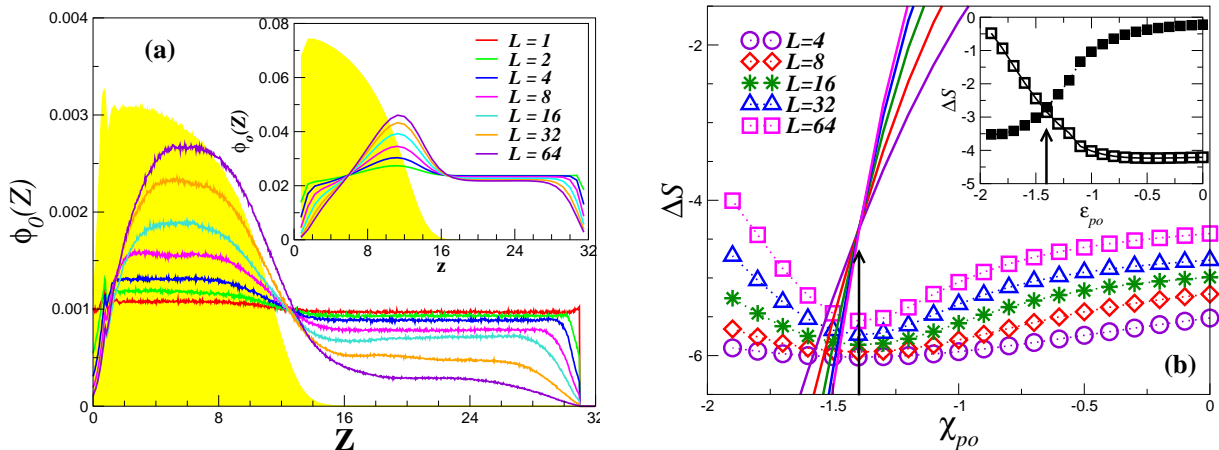


FIG. 6: (a) MC Density profiles  $\phi_0(z)$  at the “critical” strength of attraction  $\epsilon_{po}^c = 1.70$  for different lengths  $L$ . (b) SCFT results for the variation of energy (solid lines) and entropy  $\Delta S$  (symbols) of free chains of length  $L$  with changing attraction  $\chi_{po}$  to the polymer brush. Arrow indicates the intersection point of energy,  $\chi_{po}^c = -1.40$ , which coincides with the position of the minima in  $\Delta S$ . All energy values are multiplied by 10 for better visibility. In the inset the entropy  $\Delta S$  for chains with  $L = 64$  in the brush (full squares) and in the bulk (empty squares) is displayed against  $\epsilon_{po}$ .

(not shown here). Fig. 6b shows SCFT results for the excess entropy and for the internal energy per monomer (given by Eqs. (13) and (14), respectively) as a function of  $\chi_{po}$ . One notes immediately that all the energy curves intersect in a single point, corresponding to  $\chi_{po} = \chi_{po}^c$ , while all the entropy curves pass through a minimum at this point. Furthermore, the entropic curves corresponding to the polymer segments located “inside” and “outside” the brush (as defined earlier) intersect at the same value of  $\chi_{po}$  as shown in the inset of Fig. 6b.

While at  $\chi_{po}^c$  there exists thus a distance  $z$  from the grafting plane where the local concentration of polymer solutions is independent of polymer length  $L$ , provided  $\phi_{po}$  is kept constant for all  $L$ , the value of  $\chi_{po}^c$  itself is expected to depend on the concentration and/or the size of the grafted chains  $N$ . We performed SCFT calculations to see how the “critical” value of  $\chi_{po}^c$  changes with  $c_i$  and  $N$  within a broad range:  $0 \leq c_i \leq 0.375$  and  $32 \leq N \leq 256$ . We find that it increases as  $\chi_{po}^c = 1.306 + 1.326c_i + 2.393c_i^2$  with increasing free chain concentration  $c_i$ , and decreases as  $\chi_{po}^c = 1.874N^{-0.0858}$  with increasing length  $N$  of the grafted chains (in the latter case, the grafting density is adjusted such that the typical scaling variable for grafted polymers  $N\sigma_g^{1/3}$  is kept constant).

### C. Adsorption/Desorption Kinetics

Here we present our simulation and theoretical results for the kinetics of polymer adsorption/desorption into, or out of the brush. Fig. 7a shows the variation of the absorbed relative amount,  $\Gamma$ , with elapsed time  $t$  following an instantaneous switch of the interaction between brush and free chains. As expected, the expulsion of the adsorbate from the brush after an instantaneous switching off of brush - polymer attraction proceeds much faster than the absorption kinetics. The latter, as is visible from the inset to Fig. 7a, proceeds through an initial steep increase toward a saturation plateau of  $\Gamma$  whereby the small species absorb faster than those with larger  $L$ . From the intersection of the tangent to the initial steep growth of  $\Gamma$  and the saturation value one may determine the characteristic time of absorption  $\tau$  as function of  $L$  - Fig. 7b. The results are presented for all values of free chain lengths, and one sees that DDFT results are again in good agreement with kinetic MC data. This also holds in Fig. 7b where indeed the theory is in good agreement with simulations for  $N = 32$ . For the case of longer grafted chains ( $N=64$ ,  $\sigma_g=0.2$ ), no simulations were performed and only theoretical predictions are shown. Nonwithstanding, for both values of  $N$ , one clearly sees three regimes in the dependence of  $\tau$  on  $L$ . In the first regime, the absorption time grows fast and essentially linearly with  $L$  (up to  $L = 8$  for the shorter brush and  $L = 16$  for the longer one). By analyzing the data presented in Fig. 4b, one sees that this initial linear regime corresponds to the situation when  $R_g$  of absorbed chains is less than or equal to the average distance between the grafting points. As  $L$  (and, consequently,  $R_g$ ) is increased beyond the aforementioned values, one enters the second regime where the growth of  $\tau$ , while still nearly linear, is markedly slower. We interpret this slowing down as a hallmark of an increased friction of the penetrating coils when

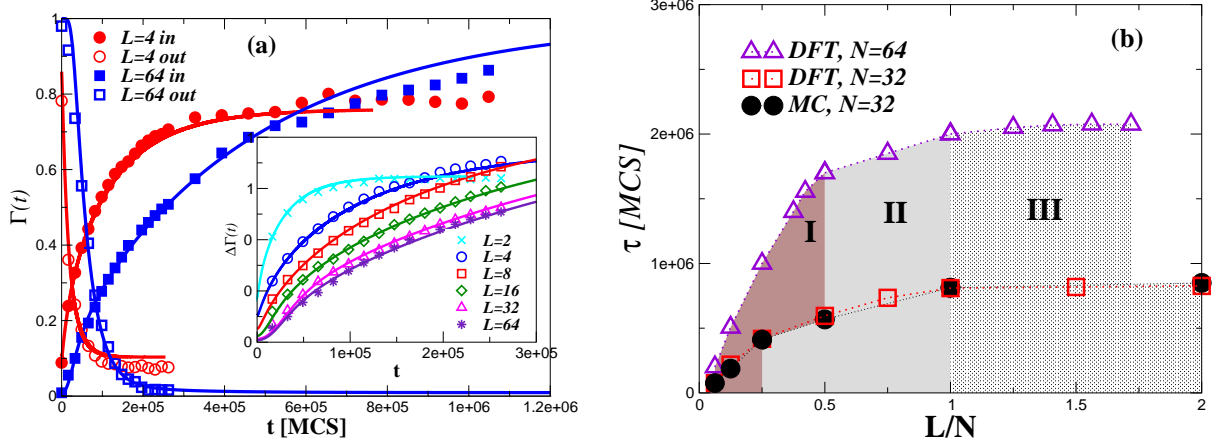


FIG. 7: (a) Variation of the absorbed amount  $\Gamma$  with elapsed time  $t$  after an instantaneous change of the interaction between brush and free chains. Here  $\sigma_g = 0.25$  and the averaging was performed over 50 cycles. The inset shows the filling kinetics for different size  $L$  of free chains. The total number of free chain monomers 512 was kept constant. (b) Absorption time  $\tau$  against polymer length  $L$  for  $\sigma_g = 0.25$  displays three distinct regimes I ( $1 \leq L \leq 8$ ), II ( $8 \leq L \leq N$ , and III ( $L > N$ ) (shaded areas).

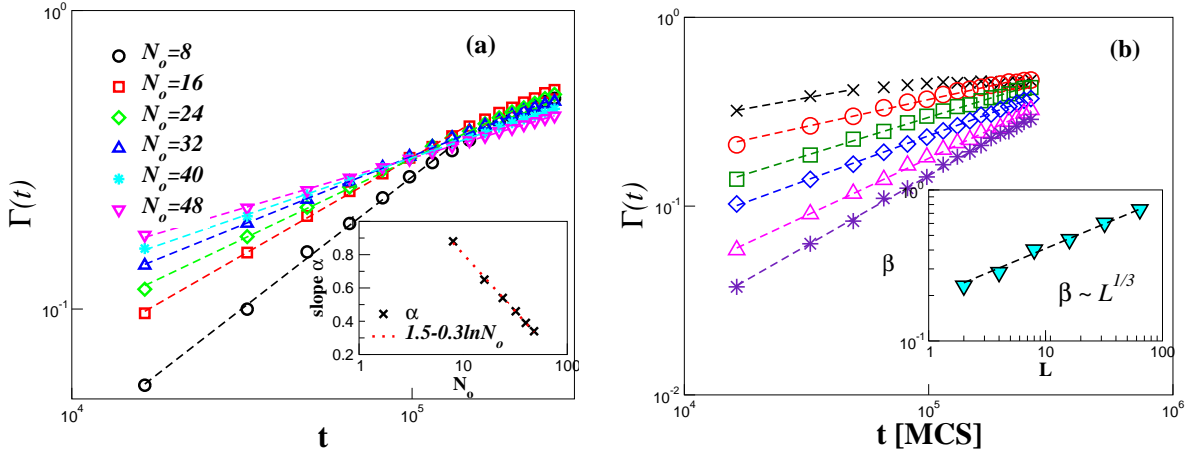


FIG. 8: (a) MC data for the absorbed amount  $\Gamma$  against elapsed time  $t$  after the onset of absorption for different concentration of free chains with  $L = 64$ . The log-log plot shows that  $\Gamma$  grows by power law  $\Gamma(t) \propto t^\alpha$ . The measured slopes  $\alpha$  are plotted in the inset against the number of free chains  $N_o$ . One finds  $\alpha \propto -\frac{1}{3} \ln \phi_o$ . (b) The same as in (a) but at the ‘‘critical’’ attraction  $\epsilon_{po} = 1.70$  and fixed  $c_i = 0.0675$  where  $\Gamma(t) \propto t^\beta$ . The exponent  $\beta \propto L^{1/3}$  (inset).

their radius of gyration exceeds the size of the cavities in the polymer brush. This regime extends up to the point where the lengths of free and grafted chains become equal. Beyond this point, for  $L > N$ , the third regime is sets in, where the absorption time is essentially independent of the free chain length. One might see therein an indication of a change in the mechanism of free chain penetration into the brush with thickness  $H < R_g$  whereby additionally the coil flattens inside the grafted layer due to gain in absorption energy.

Fig. 8a displays simulation and theoretical results for the absorption kinetics for  $N = 32$ ,  $L = 64$ , and several values of the concentration  $c_i = 64N_o/8192$ . Both MC and DDFt data show that at early and intermediate times the time dependence of the absorbed amount follows a power law  $\Gamma(t) \propto t^\alpha$ . The corresponding effective exponent  $\alpha$  is decreasing as the concentration increases (see inset), although the value of  $\Gamma$  at the beginning of the intermediate time regime is larger for larger values of  $N_o$ . This result is somewhat counter-intuitive, as one would expect the driving force for absorption (and, hence, the absorption rate) to increase with increasing concentration of free chains. A slowing down of absorption kinetics with growing size  $L$  and concentration  $c_i$  of the free chains has been experimentally

observed [62] in a porous medium (activated carbon) which resembles in certain aspects the polymer brush. In Fig. 8b we show the variation of the absorbed amount,  $\Gamma(t) \propto t^\beta$ , for the critical attraction  $\epsilon_{po} = 1.70$  - see IV B. We point out that this well pronounced power law increase of  $\Gamma$  was observed only at this particular value of  $\epsilon_{po}$  whereas for  $\epsilon_{po} = 2.00$  where most of our kinetic measurement were performed, no simple  $\Gamma - t$  relationship was found - cf. Fig. 7a. Thus, in a sense, the particular kinetics of absorption underlines the special role of the critical compatibility between brush and free chains.

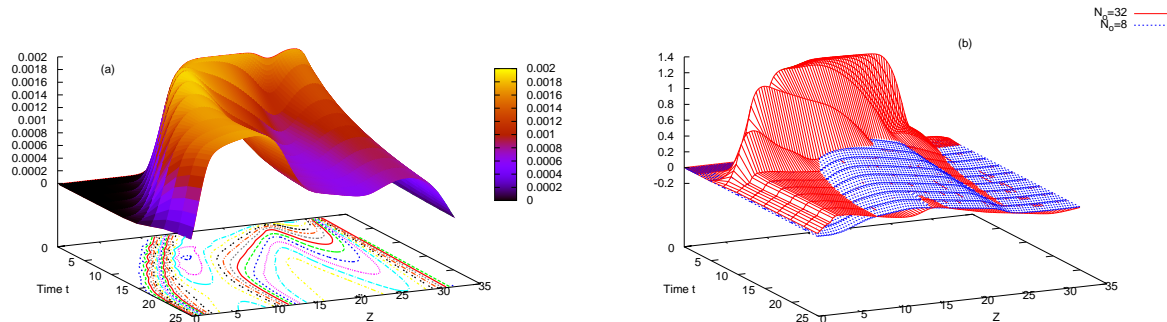


FIG. 9: (a) Changing concentration profile  $\phi_o(z)$  of free chains with time elapsed after a quench from  $\chi = 0$  to  $\chi = 2.0$  from DFT data. The time is given in logarithmic coordinates. Here the mean concentration  $c_o = 0.1875$  and the time unit corresponds to 25000 MCS. The polymer brush is located at  $0 \leq Z \leq 12.5$ . (b) Variation of the flux of free chains into the polymer brush with time for two concentrations  $c_o = 0.0625, 0.25$  i.e.,  $N_o = 8, 32$ , and  $L = 64$ .

In order to shed further light on the observed behavior, Fig. 9 shows DDFT results for the time-dependent density profile  $\phi_o(z, t)$  ( $N_o=24$ , left panel) and flux  $j(z, t)$  ( $N_o=8$  and  $32$ , right panel). In the left panel, one observes two “ridges” in  $\phi_o(z, t)$  at all times – a principal ridge, initially located in the bulk above the brush, moves gradually inside, while another (smaller) ridge is located near the opposite (bare) wall and gradually disappears still moving in the bulk. From the right panel, one can see that for higher concentration ( $N_o=32$ ) the flux prevails over the lower concentration one inside the brush and at shorter times (thereby explaining higher initial values of  $\Gamma$  seen in Fig. 8 for larger values of  $N_o$ ), while the situation is reversed outside the brush at longer times. The latter behavior is presumably due to higher mobility at lower concentrations and explains the decrease of slope  $\alpha$  with  $N_o$  seen in the inset of Fig. 8.

## V. DISCUSSION

In this work we studied a scarcely explored yet important aspect of oligomer and linear macromolecule absorption in a polymer brush - the case of (more or less) good compatibility between species in the bulk and grafted chains. Starting from oligomers (mono- and dimers) and going up to chain lengths  $L$  which exceed twice the length  $N$  of the grafted chains, we have determined the conformation of the absorbed species, the absorbed amount  $\Gamma$ , and absorption kinetics (the propagation rate into the polymer brush) at different concentration of the free chains for two cases of moderately to very dense polymer brushes. In addition, by combining Monte Carlo simulations with DFT and SCFT calculations, we have substantially broadened the range of lengths of the grafted chains to  $32 \leq N \leq 256$  in order to test more comprehensively our findings.

The most salient, and - to some extent - unexpected features of linear chain absorption in a polymer brush that we find are:

- the dramatic increase in adsorbed amount  $\Gamma(L)$  with *growing* chain length  $L$ , and
- the significant slowdown of absorption kinetics with growing concentration (i.e., with the increase of the starting gradient in density) of the free chains

Besides these static and dynamic properties of polymer absorption in brushes, we find that both the absorbed macromolecules and the brush itself largely retain their structure and conformation, as seen in quantities like  $R_g$ ,  $R_e$  and the monomer density profile  $\phi_p(z)$ , for different length  $L$  and concentration  $\phi_o$  of the free chains, and different strength  $\epsilon_{po}$  of attraction to the grafted chains. In particular, the degree to which the brush profile  $\phi_p(z)$  is affected by absorption

is found to be much less than anticipated in some earlier theoretical predictions [42]. Nonetheless, even within these small changes we observe a slight contraction of  $\phi_p(z)$  at small absorbed amounts  $\Gamma$  while  $\phi_p(z)$  gradually attains its extension roughly to that corresponding to zero concentration of free chains with growing  $\Gamma$ .

An interesting finding which still needs deeper understanding is the observed existence of a critical compatibility  $\chi^c < 0$  (i.e., brush-oligomer attraction  $\epsilon_{po}^c$ ). At  $\chi^c$  we find both in MC as well as in DFT/SCFT that the energy of all absorbed species has a value independent of their size  $L$  whereas their entropy experiences a minimum. The critical attraction  $\epsilon_{po}^c$  is manifested by the existence of a unique distance from the grafting plane where all monomer density profiles of the free chains intersect. Moreover, at  $\epsilon_{po}^c$  the kinetics of free chain absorption into the brush follows a clear cut power law with exponent  $\beta \propto L^{1/3}$ . Undoubtedly, much more work is needed until all these fascinating new features are fully understood.

Last not least, we emphasize the finding of three distinct regimes in the kinetics of free chain absorption as far as the size of the free chains  $L$  is concerned. In the first regime the characteristic time for absorption  $\tau$  grows rapidly with oligomer length  $L$  as long as the oligomer size  $R_g \propto L^\nu \approx \sigma_g^{-1/2}$  remains smaller than the separation between grafting sites. The second regime is marked by a slower increase of  $\tau$  with  $L$  and ends roughly at  $L \approx N$ . The third regime of absorption kinetics holds for  $L > N$  (i.e., the penetrating free chain cannot accommodate within the brush) and is characterized by a nearly constant  $\tau$  as far as length  $L$  is concerned. Interestingly, this rich kinetic behavior has been experimentally observed in absorption in porous media [62].

## VI. ACKNOWLEDGMENTS

One of us, (A. M.), acknowledges support under Grant No. Bi314/22. Another, (S. A. E.), acknowledges support from the Alexander von Humboldt foundation, Germany.

- 
- [1] S. Alexander, *J. Physique (Paris)* **38**, 983 (1977).
  - [2] P.-G. de Gennes, *Macromolecules*, **13**, 1069 (1980).
  - [3] A. M. Skvortsov, A. A. Gorbunov, I. V. Pavlushkov, E. B. Zhulina, O. V. Borisov, and V. A. Pryamitzyn, *Polym. Sci. USSR* **30**, 1706 (1988).
  - [4] T. Cosgrove, T. Heath, B. van Lahr, F. Leermakers, and J. M. H. Scheutjens, *Macromolecules* **20**, 1692 (1988).
  - [5] S. T. Milner, T. A. Witten, and M. E. Cates, *Macromolecules* **21**, 2610 (1988).
  - [6] M. Muthukumar and J. S. Ho, *Macromolecules* **22**, 965 (1989).
  - [7] M. Murat and G. S. Grest, *Macromolecules* **22**, 4054 (1989).
  - [8] P. Y. Lai and K. Binder, *J. Chem. Phys.* **95**, 9288 (1991).
  - [9] S. T. Milner, *Science* **251**, 905 (1991).
  - [10] A. Halperin, M. Tirrell, and T. P. Lodge, *Adv. Polym. Sci.* **100**, 33 (1992).
  - [11] I. Szleifer and M. A. Carignano, *Adv. Chem. Phys.* **94**, 165 (1996).
  - [12] J. Klein, *Ann. Rev. Mater. Sci.* **26**, 581 (1996).
  - [13] G. S. Grest and M. Murat, in *Monte Carlo and Molecular Dynamics Simulations in Polymer Science*, Ed. K. Binder, Oxford Univ. Press, New York, 1995, pp. 476-578.
  - [14] G. S. Grest, *Adv. Polym. Sci.* **138**, 149 (1999).
  - [15] L. Leger, E. Raphael, and H. Hervet, *Adv. Polym. Sci.* **138**, 185 (1999).
  - [16] *Polymer Brushes*, Eds. R. C. Advincula, W. J. Brittain, K. C. Caster, and J. R uhe, Wiley - VCH, Weinheim, 2004.
  - [17] D. H. Napper, *Polymeric Stabilization of Colloidal Dispersions*, Academic Press, London, 1983.
  - [18] H. R. Brown, *Mat. Res. Soc. Bull.* **21**, 24 (1996).
  - [19] G. Storm, S. O. Belliot, T. Daemen, and D. D. Lasic, *Adv. Drug. Deliv. Res.* **17**, 31 (1995).
  - [20] A. Hucknall, A. J. Simmick, R. T. Hill, A. Chieboli, A. Garcia, M. S. Johannes, R. L. Clarck, S. Zaucher, and B. D. Ratner, *Biointerfaces* **4**, FA50 (2009).
  - [21] A. J. Wang, J. J. Xu, and H. Y. Chen, *J. Chromatography, A* **1147**, 120 (2007).
  - [22] J. U. Kim and B. O. O'Shaughnessy, *Macromolecules* **39**, 413 (2006).
  - [23] D. I. Dimitrov, A. Milchev, K. Binder, *J. Chem. Phys.* **127**, 084905 (2007).
  - [24] A. Halperin, G. Fragneto, A. Schollier, and M. Sferrazza, *Langmuir*, **23**, (2007).
  - [25] S. A. Egorov, *J. Chem. Phys.* **129**, 064901 (2008).
  - [26] J. Yaneva, D. I. Dimitrov, A. Milchev and K. Binder, *J. Colloid Interface Sci.* **336**, 51 (2009).
  - [27] D. Trombly and V. Ganesan, *J. Polym. Sci. B* **47**, 2566 (2009).
  - [28] D. Dukes, Y. Li, S. Lewis, B. Benicewicz, L. Schadler, and S. K. Kumar, *Macromolecules* **43**, 1564 (2010).
  - [29] E. P. Currie, J. van der Gucht, O. V. Borisov, and M. A. Cohen-Stuart, *Langmuir* **14**, 5740 (1998).
  - [30] K. Chen and Y. A. Ma, *J. Phys. Chem. B* **109**, 17617 (2005).
  - [31] J. U. Kim and M. W. Matsen, *Macromolecules* **41**, 246 (2008).

- [32] A. Milchev, D. I. Dimitrov and K. Binder, *Polymer* **49**, 3611 (2009).
- [33] S. Gupta, M. Agraval, P. Uhlmann, F. Simon, U. Oetel, and M. Stamm, *Macromolecules* **41**, 8152 (2008).
- [34] A. P. Gast, L. Leibler, *Macromolecules*, **19**, 686 (1986).
- [35] H. R. Brown, K. Chare, and V. R. Deline, *Macromolecules* **23**, 3383 (1990).
- [36] T. Witten, L. Leibler, and P. Pincus, *Macromolecules*, **23**, 824 (1990).
- [37] E. B. Zhulina, O. V. Borisov, L. Brombacher, *Macromolecules*, **24**, 4679 (1991)
- [38] C. M. Wijmans, E. B. Zhulina, and G. J. Fleer, *Macromolecules*, **27**, 3238 (1994); C. M. Wijmans and B. J. Factor, *Macromolecules*, **29**, 4406 (1996).
- [39] M. Aubouy, E. Raphael, *Macromolecules*, **27**, 5182 (1994);
- [40] J. I. Martin and Z. G. Wang, *J. Phys. Chem.* **99**, 2833 (1995).
- [41] M. P. Pepin and M. D. Whitmore, *J. Chem. Phys.* **114**, 8181 (2001).
- [42] I. Borukhov and L. Leibler, *Macromolecules* **35**, 5171 (2002)
- [43] H. Huang, A. Cammers, and L. S. Penn, *Macromolecules*, **39**, 7064 (2006).
- [44] R. Yerushalmi-Rosen, J. Klein and L. J. Fetters, *Science* **263**, 793 (1994).
- [45] C. J. Clarke, R. A. L. Jones, J. L. Edwards, K. R. Shull, and J. Penfold, *Macromolecules* **28**, 2042 (1995).
- [46] G. Reiter, P. Auroy, and L. Auvray, *Macromolecules* **29**, 2150 (1996).
- [47] M. Müller and L. G. MacDowell, *Europhys. Lett.* **55**, 221 (2001).
- [48] S. Jain, V. V. Ginzburg, P. Jog, J. Weinhold, R. Srivastava, and W. G. Chapman, *J. Chem. Phys.* **131**, 044908 (2009).
- [49] F. Pierce, D. Perahia, and G. Grest, *Macromolecules* **42**, 7969 (2009)
- [50] P. Y. Lai, *J. Chem. Phys.* **98**, 669 (1999).
- [51] A. Kopf, J. Baschnagel, J. Wittmer, and K. Binder, *Macromolecules* **29**, 1433 (1996).
- [52] J. Wittmer, A. Johner, J. F. Joanny, and K. Binder, *J. Chem. Phys.* **101**, 4397 (1994).
- [53] P. Flory, *Principles of Polymer Chemistry*, Cornell University Press, Ithaca, 1953.
- [54] M. Borowko, W. Rzyso, S. Sokolowski, and T. Staszewski, *J. Phys. Chem. B* **113**, 4763 (2009)
- [55] Milchev A, Paul W, Binder K, *J. Chem. Phys.* **99**, 4786 (1993).
- [56] Milchev A, Binder K. *Macromol. Theory Simul.* **5**, 915 (1994)
- [57] S. Semal, M. Vou, M. J. de Ruijter, J. Dehuit, and J. De Coninck, *J. Phys. Chem. B* **103**, 4854 (1999).
- [58] A. Milchev, K. Binder, *Macromolecules* **29**, 343 (1996).
- [59] A. Milchev, K. Binder, *J. Chem. Phys.* **114**, 8610 (2001).
- [60] A. Yethiraj and C. E. Woodward, *J. Chem. Phys.* **102**, 5499 (1995).
- [61] C. E. Woodward, *J. Chem. Phys.* **94**, 3183 (1991).
- [62] H. D. Do, D. D. Do, and I. Prasetyo, *AIChE J.* **47**, 2515 (2001).
- [63] J. G. E. M. Fraaije, *J. Chem. Phys.* **99**, 9202 (1993).
- [64] H. Xu, H. Liu, and Y. Hu, *Chem. Eng. Sci.* **62**, 3494 (2007).
- [65] B. M. Steels, J. Koska, and C. A. Haynes, *J. Chromatography B*, **743**, 41 (1991).
- [66] R. Roth, *J. Phys. Cond. Matt.* **22**, 063102 (2010).